

P. Franzen, J. Sielanko, H.P.L. De Esch, E. Speth,
B. Heinemann, R. Riedl

**Design Studies for an Alternative Magnetic Residual
Ion Removal System for the ITER Neutral Beam
Injection System**

Design Studies for an Alternative Magnetic Residual Ion Removal System for the ITER Neutral Beam Injection System

P. Franzen, J. Sielanko[†], H.P.L. De Esch[‡], E. Speth, B. Heinemann, R. Riedl

*Max-Planck-Institut für Plasmaphysik, EURATOM Association, POB 1533,
D-85740 Garching, Germany*

*[†]Uniwersytet Marii-Curie Skłodowskiej, Pl. Marii Curie-Skłodowskiej 5,
20-031 Lublin, Poland*

[‡]CEA Cadarache, 13108 St Paul Lez Durance, France

IPP 4/281

March 2003

Dieser IPP-Bericht ist als Manuskript des Autors gedruckt. Die Arbeit entstand im Rahmen der Zusammenarbeit zwischen dem IPP und EURATOM auf dem Gebiet der Plasmaphysik. Alle Rechte vorbehalten.

This IPP-Report has been printed as author's manuscript elaborated under the collaboration between IPP and EURATOM on the field on plasma physics. All rights reserved.

Abstract

An alternative residual ion removal concept for the ITER neutral beam system is presented. It consists of magnetic deflection of the residual ions to in-line ion dumps. The target plates are hit from one side and form a 0.5 m wide opening to the beam. First calculations show that for the most severe case of a 3-mrad beam the maximum power load can be kept below 15 MW/m^2 , using a re-optimized horizontal focal length. First calculations showed that using a passive screening the additional stray field created by the magnet could be kept below the required 1 Gauss within the neutralizer. The overall beamline transmission increases by about 10% (i.e. additional 1.7 MW injected power for each beamline for a 3-mrad beam) due to the open structure of the magnet and the ion dumps. Furthermore, the concept offers a much larger operating window regarding beam alignment, divergence, steering and transmission and it avoids creating accelerated secondary electrons.

Contents

1	Introduction	9
2	Present design of the ITER neutral beam line	9
3	Calculations	11
4	Previous Concept Studies of MIRS.....	13
4.1	Vertical Deflection	14
4.2	Horizontal deflection	14
4.2.1	90° deflection to remote dump plates.....	14
4.2.2	180° deflection to remote dump plates.....	15
5	Final Concept.....	16
5.1	Magnet and Dump Design	17
5.2	Screening.....	17
5.3	Power Deposition on the Dump Plates	19
5.4	Parameter studies.....	20
5.4.1	Magnet position.....	21
5.4.2	Focal lengths / Grid optics.....	21
6	Beamline Transmission (by H.P.L De Esch)	24
6.1	Perveance scans	25
6.2	Results of the calculations	26
7	Summary	27
	References	28

1 Introduction

The present reference design [1] of the residual ion dump system for the neutral beam injection (NBI) system of ITER is based on electrostatic deflection of the residual ions (about 40% of the extracted power at 1 MeV, with roughly equal power fractions for D^+ and D^- ions) to in-line dump plates. This electrostatic residual ion dump (ERID) forms four narrow channels (1.8 m long and 0.9 m wide at the exit) corresponding to the grounded grid geometry. The plates are alternatively biased with about 25 kV. This concept has the advantage of a simple and compact design and it generates no additional magnetic stray field.

However, such a concept has never been used in any working NBI system. All systems — positive ion based (see for example ASDEX Upgrade [2],[3], W7-AS [4], JET [5], TFTR [6], JT-60U [7], DIII-D [8]) as well as negative ion based (LHD [9], JT-60U [10]) — use a magnetic deflection system with remote ion dumps in order to avoid accelerating secondary electrons [11] and beam blocking due to a possible increased pressure in the dump channels. Furthermore, lifetime considerations [12] of the swirl tubes used for the ion dumps in the reference design which have to be fed with the cooling water from the top showed that power sweeping is necessary in order to reduce the power load to the acceptable value of 6 MW/m^2 . These power load restrictions and the narrow channels of the ERID result in a small operating window with respect to beam alignment, steering and beamlet divergence, i.e. the beam optics.

Due to these disadvantages of ERID, an alternative concept consisting of magnetic deflection of the residual ions was studied. The concept of such a magnetic ion removal system (MIRS) is straightforward: the residual positive and negative ions are deflected upwards and downwards by a horizontal magnetic field or are deflected sideward by a vertical magnetic field. Due to the limited space and the geometric restrictions of the ITER beamline design, only 90° deflection is possible — the preferred 180° deflection, as it is the case in many of the present neutral beam systems, requires beamline dimensions at least three times larger than the beam dimensions; hence, focusing effects dominate the power deposition profiles in the case of 90° deflection rendering this approach less favorable.

In the following, after a short section regarding the calculations, several different concepts of such a magnetic ion removal system are discussed. As a result of these studies, the final concept of a magnetic ion removal system is presented consisting of sideward magnetic deflection, but to in-line vertical dump plates, as in the electrostatic case. The ions hit the target plates only from one side with oblique incidence. In this report, the results of a 'proof-of-concept' study of such a system are presented, the final detailed design, however, needs further work.

2 Present design of the ITER neutral beam line

Figure 1 and Figure 2 show the present design of the ITER NBI system. Indicated is the space allocated for the residual ion removal system [13] (presently occupied by ERID). Also shown is the space that is needed for the final design of MIRS using the beam focusing parameters of the reference design (see below). The available space is determined by the neutralizer and the calorimeter in x -direction and by the cryopump and the beam in y - and z -direction. (The coordinate system used in this paper is indicated in Figure 2, the x -axis is defined by the beam axis, the grounded

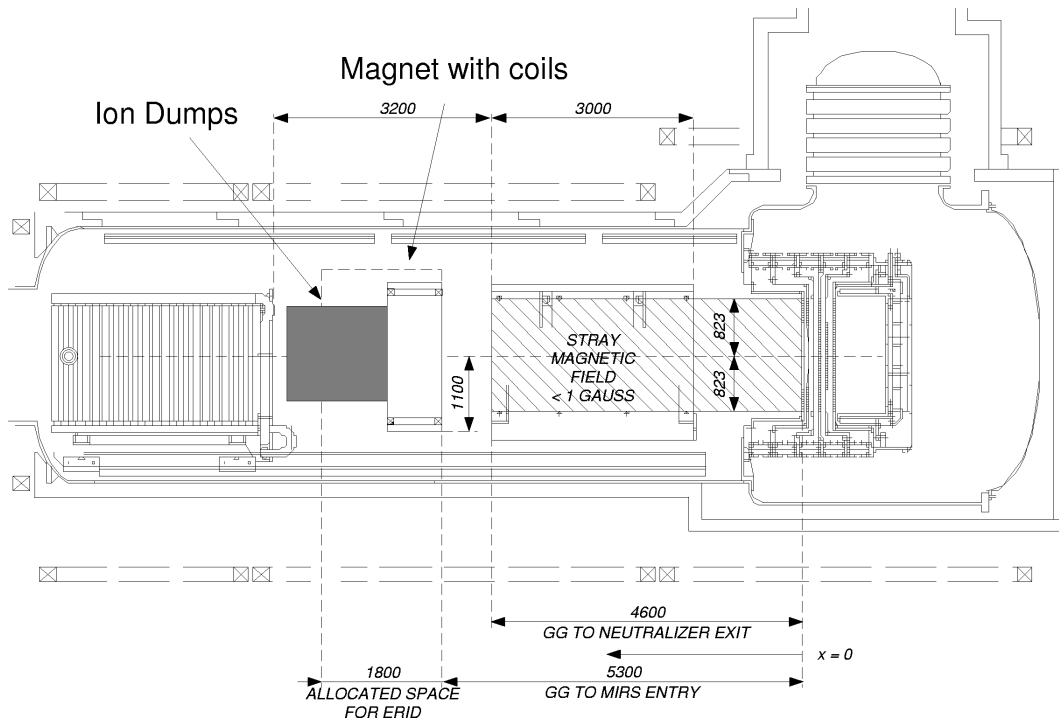


Figure 1: ITER neutral beam design. Dimensions are given in mm. The dashed line indicates the space presently allocated for the electrostatic residual ion system. Also indicated is the space needed for the magnet and the dump plates of the magnetic ion removal system (MIRS) that is discussed in this paper.

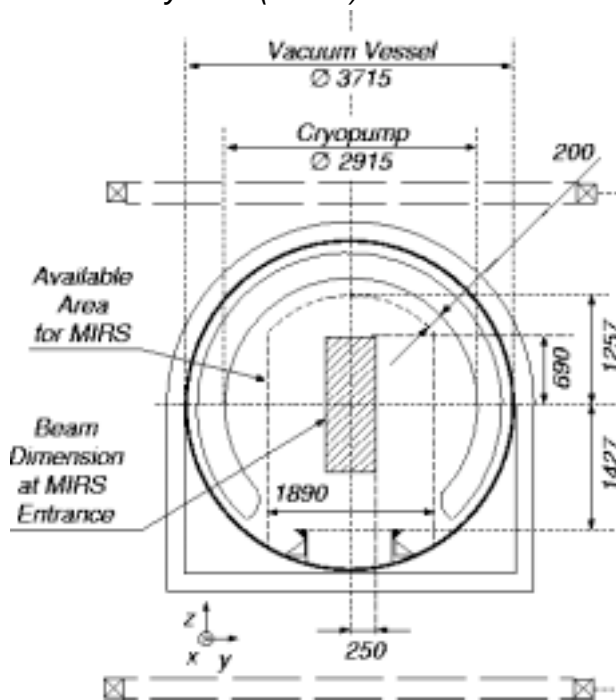


Figure 2: Available Space for the MIRS [13] (as it is allocated for ERID in the present design) with the coordinate system. The grounded grid defines $x=0$. Dimensions are given in mm. The available space in x -direction ranges from 5.3 m to 7.1 m.

grid being located at $x = 0$.) The neutralizer exit is located at $x = 4.6$ m, the entrance of the calorimeter is located at $x = 7.8$ m.

There are large gaps between the neutralizer and the ERID (0.7 m) as well as between the ERID and the calorimeter (also 0.7 m), which allows sufficient pumping to minimize the re-ionization losses in the beamline. A further requirement is that the total stray field inside the neutralizer from the magnet and the tokamak has to be below 1 Gauss; this is due to the fact that the 4 groups of beamlets are aligned to the segmented neutraliser.

The grounded grid of the reference design consists of 1280 beamlets (see Table 1) with a radius of 7 mm. The grid is subdivided in 16 subgrids arranged in a 4x4 matrix with horizontal seg-

Table 1: Beam parameters of the present ITER NBI design

Beam particles and energy:	Deuterium, 1 MeV
Total accelerated current:	40 A
Ion fractions to RID's:	20% D ⁻ , 20% D ⁺
Beam divergences:	3 mrad, 5 mrad, and 7 mrad with a 15%, 15 mrad halo
Number of vertical grid segments:	4
Number of horizontal grid groups:	4
Number of beamlets per subgrid:	5 x 16 = 80
Total grid dimensions:	0.58 x 1.54 m ²
Segments vertical and groups horizontal aiming point:	23.4 m from grounded grid
vertical focal length of a subgrid:	∞
horizontal focal length of a subgrid:	7.1 m

ments and vertical columns. Each subgrid consists of 5x16 beamlets; the distance between the individual beamlets is 22 mm in vertical direction and 20 mm in horizontal direction, respectively. The columns are separated by 80 mm, the segments by 66 mm. Both the vertical columns and the horizontal segments aim to the narrowest place of the beamline, i.e. the duct exit at 23.4 m. Furthermore, the beamlets of each subgrid are focused horizontally by offset steering to the exit of the ERID at 7.1 m (see also Figure 18 below).

3 Calculations

The power density profiles on the ion dumps have been calculated by means of a 3D Monte Carlo code based on the TRHN program [14], using a 3D 'real' magnetic field distribution. This was calculated with the code PROFI [15]. Similar codes have been also used for the design of the ASDEX long pulse injection system and the ASDEX Upgrade residual ion dump system and gave results in good agreement with experiments [16].

Table 1 summarizes the beam parameters used in the calculations. The divergences correspond to the set of divergences in the ITER NBI reference design [13]. A large number of ions (120,000) with random starting points and directions depending on focusing and divergence are followed until they hit predefined surfaces. For reasons of simplicity, the calculations were performed for the positive ions only. Space charge effects can be neglected, as a comparison of results including and excluding space charge corrections has shown. These corrections take the full interaction of the positive ions into account, but not the compensation due to the negative ions and the background residual gas.

The typical 2D grid of the (virtual or real) plane where the power is deposited has 46x64 pixels, with typical dimensions of 50 to 60 mm in x-direction, 15 to 20 mm in y-

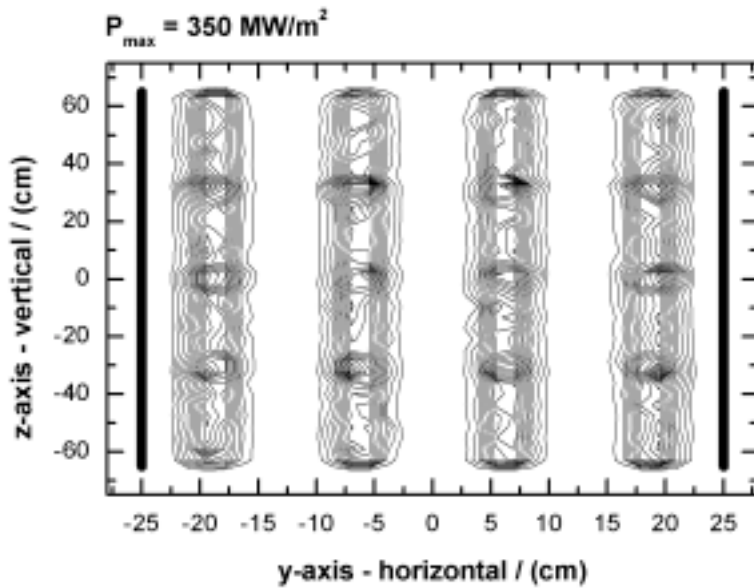


Figure 3: Beam profile at the entrance of the magnet ($x = 5.3$ m) for the beam parameters given in Table 1. The divergence is 3 mrad. The lines are drawn in steps of 25 MW/m^2 . The maximum power density is of the order of 350 MW/m^2 ; the total power is 40 MW. Note the different scaling of the z- and y-axis.

reference design [1], [12] (not shown in this paper).

Figure 3 shows the resulting beam profile — consisting both of neutrals (60%) and ions (40%) — at the entrance of the ion deflection system (ERID or MIRS, respectively) at $x = 5.3$ m. The beam parameters are given in Table 1; the divergence is 3 mrad. The maximum beam power (neutrals and ions) is of the order of 350 MW/m^2 with a total power of 40 MW (beam losses in the neutralizer are neglected). However, these maximum power loads are concentrated in a few hot spots; these spots are a result of the design of the grid optics: there is a vertical overlap of the beamlet groups within a column due to the focusing, aiming and divergence of the beamlets. This overlap is less pronounced for larger divergences (not shown here).

As can be seen from Table 1, about 40% of the beam particles leaving the neutralizer are ions; hence the residual ion removal system has to handle about 16 MW with equal amounts for the positive and negative residual ions, respectively. (This is the case if the neutralizer target thickness is near the optimum value; otherwise the ion fractions are not balanced. This might be a problem for the power supplies of ERID.) The maximum power density has to be reduced from $0.2 \times 350 \text{ MW/m}^2 = 70 \text{ MW/m}^2$ to acceptable values, say below 15 MW/m^2 , which can be handled by target plates.

The design of the magnet as well as the coil currents are changed until the power density has come to these acceptable values. The magnet and ion dump designs presented in this paper are the result of a iteration between selecting a magnet design, calculating the field distribution and the power deposition profile on a virtual plate, selecting a ion dump design and calculating the power deposition profile on the 'real' dump plates, until the power load is sufficiently low. So far only a global dump surface has been defined without any attempt of subdividing it in individual Hypervatron [5] or ASDEX Upgrade [17] type panels. This can be done, when the final dump design is chosen.

direction and 25 to 30 mm in z-direction. The error due to the statistical nature of the calculations can be estimated from the total integral of the power deposition profile onto a real or virtual plane, i.e. the total power. In all cases this integral was within $\pm 5\%$ of the nominal power. So the power deposition profiles will be within that error for larger areas (say 10 pixels). However, the error in the maximum power density may be larger; consecutive runs showed an agreement within $\pm 10\%$. The code has also been checked by calculating the power deposition profiles for electrostatic deflection. The results agree very well with those of the

4 Previous Concept Studies of MIRS

In this section the several MIRS concepts that have been developed in the last years are discussed:

Case 1: 90° vertical deflection to more or less remote ion dumps,

Case 2: 90° horizontal deflection to remote ion dumps,

Case 3: 180° horizontal deflection to remote ion dumps,
and finally,

Case 4: horizontal deflection to in-line ion dumps with oblique incidence.

Due to the smaller gap between the magnet coils, case 1 was studied first. (The details can be found in a previous paper [18].) The ions are deflected by a horizontal magnetic field up- and downwards. However, this concept as well as other concepts with more or less remote ion dumps have several drawbacks that are discussed below. Due to limited space especially above the beam — 0.4 m to 0.6 m free space to the cryo pump — only 90° deflection is possible. With this deflection to almost 90°, the residual ion beam is strongly focused, leading to very high power densities. This, however, is a common feature of magnetic reflection within a real non-uniform field.

Furthermore, these effects depend very critically on beam alignment, divergence and steering.

In contrast, case 2 — deflection of the residual ions to the left and right side of the beam to remote ion dump — may offer some advantages due to the larger distance of the beam to the cryopump (0.65 m, being slightly larger than the beam width), in spite of the larger gap between the magnet coils. As can be seen below this concept includes simple slightly inclined target plates of both sides of the beam. But again, due to 90° deflection, this concept also suffers from focusing.

Due to these focusing limitations the possibility of a 180° deflection design (case 3) was also investigated — in spite of the space limitations mentioned above. However, as discussed below, not all of the ions are bent by 180°, so that focusing still plays a role; and, furthermore, the still limited space at the sides of the beam especially at the upper and lower beam edges does not allow a design with sufficiently low power density.

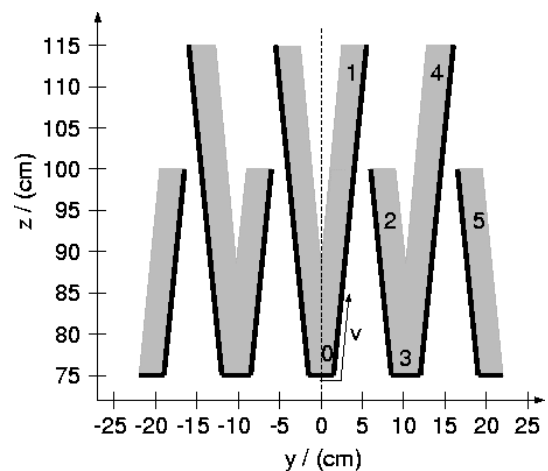
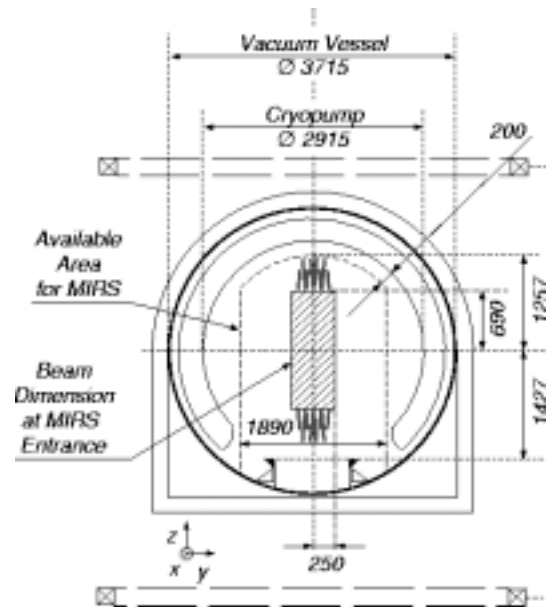


Figure 4: Design for vertical deflection to remote ion dumps.

The final solution (case 4) with sufficient low power deposition onto the target plates is the concept of an oblique deflection to in-line target plates. This design is thoroughly discussed in Section 5.

4.1 Vertical Deflection

Figure 4 shows the ion dump design for vertical ion deflection. In order to avoid a strong focusing towards the sidewalls of the magnet (in y direction) due to the fringe field, a magnet geometry with two coils at each side has been chosen (For details see [18]). The magnetic field increases in steps from 0.1 T to 0.35 T at the end of the magnet. The fringe field at the coils exceeds 1 T.

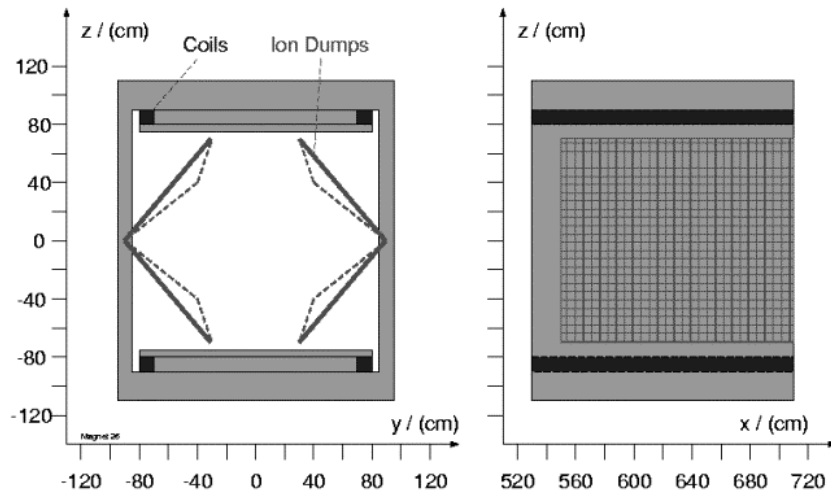


Figure 5: Magnet and ion dump design for horizontal deflection. The solid and broken lines indicate two different dump designs, respectively.

The design of the ion dumps was very carefully adapted to the grid geometry. The total dump area is about 7 m^2 . The target plates have been designed for a beam with 3-mrad divergence, and for that case the maximum power load can be kept below 25 MW/m^2 . This power density, however, exceeds the limit of 15 MW/m^2 that can be handled with large area Hypervapotron plates. Furthermore, the horizontal plates between the ‘hats’ receive a power load of more than 65 MW/m^2 for the low divergence case; this is not tolerable.

As already discussed above, this ‘four hat’ design has the disadvantage of being aligned to the actual grid design and beam parameter (tilting, focusing, misalignment and divergence). Especially the limited space above the beam (only about 0.55 m with a beam height of about 1.3 m) limits the inclination angle and the available area for an ion dump. In the latest design upgrade of ITER NBI, the vertical steering angle of the ion source is variable in order to change the power deposition in the plasma. Hence, vertical deflection — as it was designed before the introduction of a variable steering — is not possible.

4.2 Horizontal deflection

4.2.1 90° deflection to remote dump plates

Figure 5 shows a first design of a magnet and dump plates for 90° horizontal deflection. The dumps are again v-shaped. The magnet is simpler as in the case of vertical deflection, having only one coil at top and bottom, respectively. Due to the large distance of the coils to the beam in y -direction (the beam ends at y about 25 to 30 cm, and the coil is located at $y = 70$ cm), the residual ions travel through a relatively homogeneous magnetic field of only 0.05 T. This leads to a weak power density enhancement by focusing, as can be seen in the fact that the maximum power density at the virtual vertical plate at $y = \pm 30$ cm, is only about 35 MW/m^2 (not shown here),

and that this power density increases only slightly with increasing distance to the neutral beam.

Also indicated in Figure 5 are two first very preliminary ion dump designs. The total area of the dumps is again about 7 m². Figure 6 shows the power deposition profiles for the two target designs. The maximum power load is in both cases below 26 MW/m² for a beam with 3-mrad divergence. In contrast to the design for vertical deflection above, the maximum power density decreases with increasing divergence. As can be seen in the top picture of Figure 6, the power density can be reduced by a proper design of the target plates. However, this design needs still an ion dump reaching beyond the limit of $x = 7.1$ m.

This horizontal deflection concept has the advantage that an adaptation to the grid design and beam parameters is not that mandatory as in the case above.

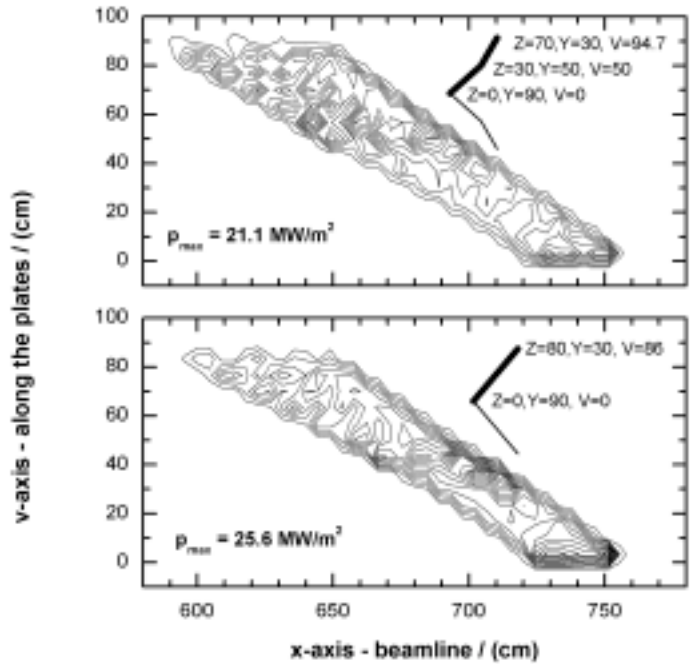


Figure 6: Power deposition profiles for the two different ion dump designs (see Figure 5). The lines are drawn in steps of 2 MW/m². The divergence is 3 mrad. Shown is only the upper half of the dump.

4.2.2 180° deflection to remote dump plates

As already mentioned above, 180° deflection to remote ion dumps requires beamline

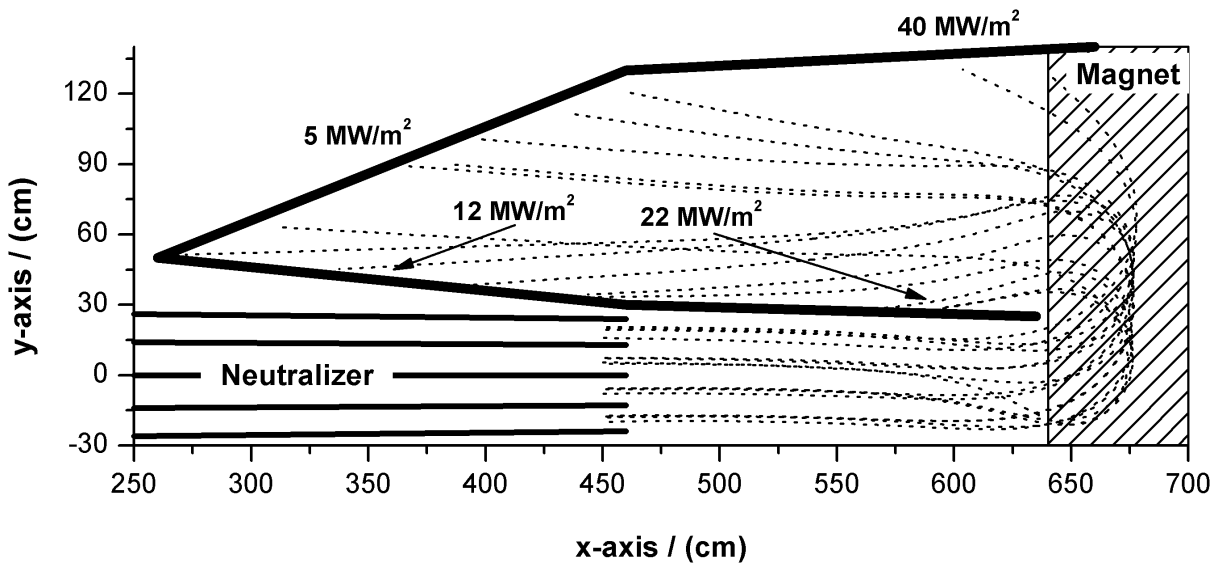


Figure 7: Example of a design for 180° deflection. The trajectories are projections to the xy -plane. Only a few trajectories of 120000 are shown. Different starting points in z -direction cause the different bending radii.

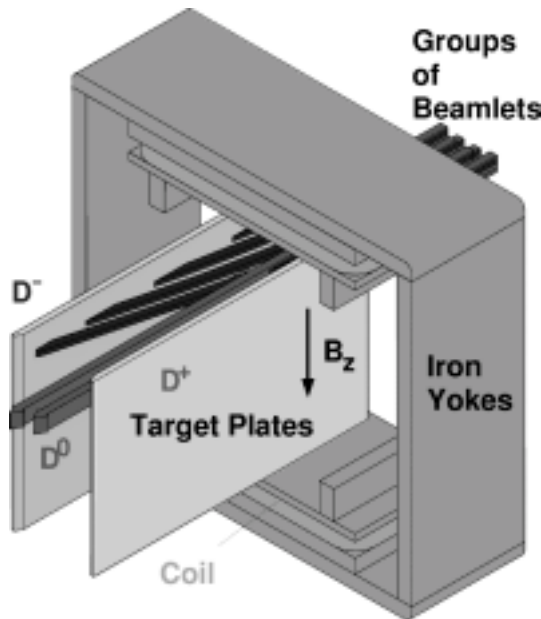


Figure 8: 3D view of the magnet and the ion dumps of the final MIRS design. The vertical magnetic field is about 0.4 T.

dimensions at least three times larger than the beam dimensions. As can be seen in Figure 2, this is the case horizontally at least in the $z = 0$ plane.

As a proof-of-concept study — which also might prove that the concept is not possible — we investigated the following setup (see Figure 7):

- a magnet with dimensions of $\Delta x = 0.6$ m, $\Delta y = 2.6$ m, $\Delta z = 1.8$ m, respectively;
- the ions are mostly bent within the magnet by 180° by a magnetic field of 0.8 T;
- the magnet is located at $x = 6.4$ m;
- and a v-shaped dump with 4 plates and a total length of 4 m, starting at $x = 2.6$ m; this is beneath the neutralizer. The horizontal width of the dump is about 1.15 m.

The first calculations showed that this concept suffers still from the space limitations, especially near the upper and lower edges of the beam. Here the free space within the cryo pump is very narrow.

Figure 7 shows the results of a first calculation. The maximum power loads even for this large ion dump is still of the order of 40 MW/m^2 , this is at the edge of the ion dump where the ions from the beam edge are bent by almost 90° . The total length of the dump is nearly 8 m; the total dump area is $2 \times 12 \text{ m}^2$. The beam dimensions are too large and the free space within the beamline too small in order to bend all the ions with 180° . Hence, again focusing effects play an important role and this concept was also abandoned.

5 Final Concept

All the concepts for a magnetic ion removal system that have been discussed in the previous section suffer from space limitations and — more or less — focusing effects due to the 90° deflection.

In this section the final concept is presented. Figure 8 shows a 3D drawing of the design with the magnet and the ion dumps. This concept consists of still sideward deflection, but to in-line dump plates, as in the case of electrostatic deflection. However, in this case only two plates are needed instead of five, and the plates are hit only from one side. This reduces the area receiving the ion power of 16 MW by a factor of 4. The total dump area is again about 7 m^2 . The plates can be fed with cooling water from the rear, instead of feeding from the top (ERID). This higher freedom of the cooling design enables the plates to handle much more power density than the ERID swirl tubes plates with a maximum power capacity of only 6 MW/m^2 . There is no final design of the target plates and no estimation of the maximum power density the targets can handle. Hence we assume an upper limit of 15 MW/m^2 .

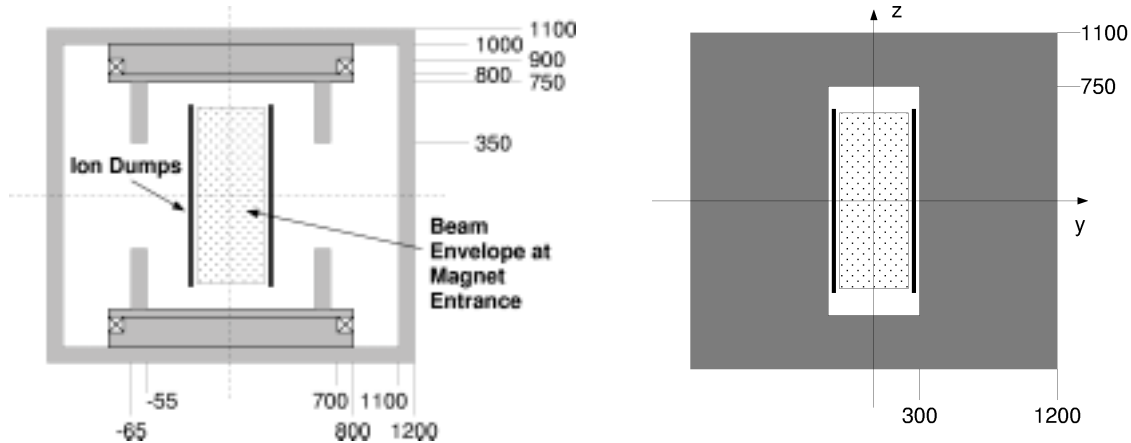


Figure 9: Magnet configuration (without screening) used in the calculations. The crosses indicate the coils. The magnet body consists of ARMCO iron. Dimensions are given in mm. The magnet starts at 5.3 m and is 0.8 m long. The maximum magnetic field in z-direction is -400 Gauss. Also indicated are the position of the dump plates and the beam envelope at the entrance of the magnet.

5.1 Magnet and Dump Design

Figure 9 shows the detailed magnet design. The magnet is located at $x = 5.3$ m and is 0.8 m long. The design of the 'outer cage' of the magnet is not yet adapted to the ITER beam geometry. The legs have been introduced in order to improve the homogeneity of the magnetic field distribution in the beam area. The coils consist of 4 turns each and are fed with 9 kA per coil.

The dump plates are located as near to the beam as possible — at $y = -0.25$ m and $+0.25$ m, respectively —, in order to minimize focusing effects (see above) and to keep the incident angle as low as possible. The two plates start inside the magnet — at the magnet entrance — and are roughly 1.5 m high and 2.2 m long and present a 0.5 m wide opening to the beam. The total area of the target plates is 2×3.3 m².

An important result of the calculations was that the power deposition profiles do not depend very critically on the detailed design of the magnet. This means also that our design is rather robust against beam misalignment and changes of the beam steering.

5.2 Screening

As already mentioned above, the neutralizer design — with four channels for the grid segment — requires that the magnetic stray field in the neutralizer region is below 1 Gauss. The stray field of the tokamak is screened by six correction coils (see Figure 1) below and above the beamline outside the vacuum vessel. Although it might be possible to screen also the stray field of the magnet with these external

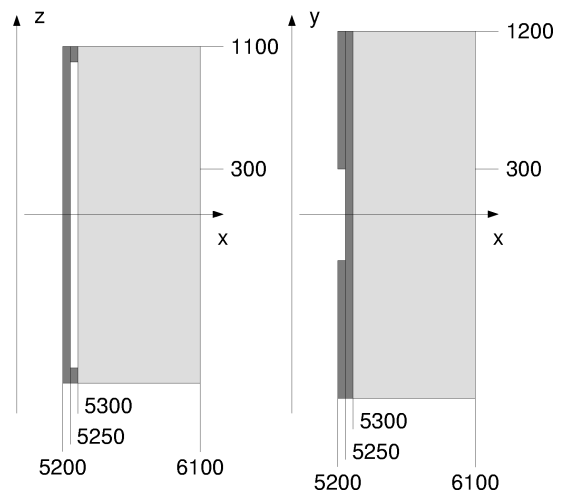


Figure 10: Screening of the magnet (see Figure 9)

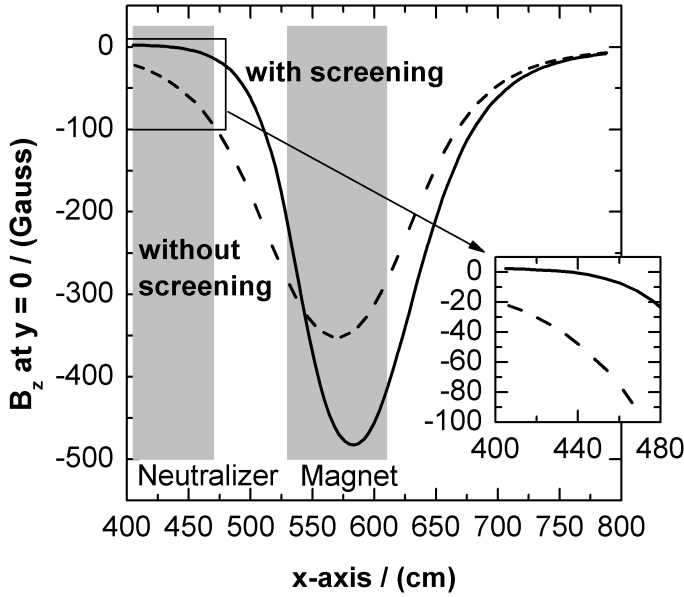


Figure 11: Vertical magnetic field strength at $z = 0$ and $y = 0$ along the beamline axis for a screened magnet compared to an unscreened.

neutralizer exit is strongly reduced compared to the unscreened magnet; furthermore, the maximum field strength is larger (-500 Gauss compared to -350 Gauss) and is shifted by a few centimeters. This different magnetic field strength has consequences for the power density profiles onto the target plates (see below).

As already mentioned above, the limit of 1 Gauss inside the neutralizer is because of the alignment of the beamlet groups to the segmented neutralizer in order to minimize the losses at the neutralizer plates. However this limit is meaningful for the tokamak stray field: it is nearly constant in the neutralizer region, which is 20 m away from the field coils. For a rapidly changing field as it is the case for MIRS, the field distribution inside the neutralizer has also to be taken into account. This can be done by requiring that the integral of the magnetic field must be a certain value. This gives in zero order at $y=0, z=0$, where the field has a maximum, a limit of

$$\int_{\text{Neutralizer}} B dx < 1 \text{ Gauss} \times 3 \text{ m} = 3 \text{ Gauss m},$$

coils, however with implications on the bending field, we studied the possibility of a passive screening by ferromagnetic materials alone. The investigations are in a very preliminary state, however, general trends can be seen.

Figure 10 shows an example of a very preliminary arrangement of the screening. It consists of 10 mm thick plates made out of ARMCO material. These plates close the magnetic field lines in front of the magnet. The resulting magnetic field strength in the center of the beamline (i.e. at $y = 0$ and $z = 0$, respectively) is compared with the unscreened case in Figure 11. The currents in the coils are equal in both cases. The magnetic field strength at the neu-

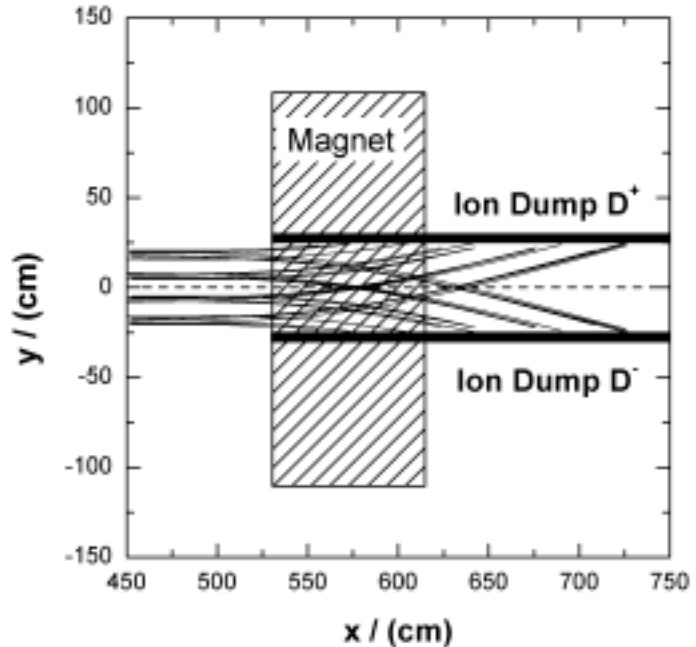


Figure 12: Residual ion trajectories hitting the dump plates indicated in Figure 9 for a 3 mrad, 1 MeV beam with the design parameters. The magnet is not screened. The maximum angle of incidence is about 14° for the outermost beamlets.

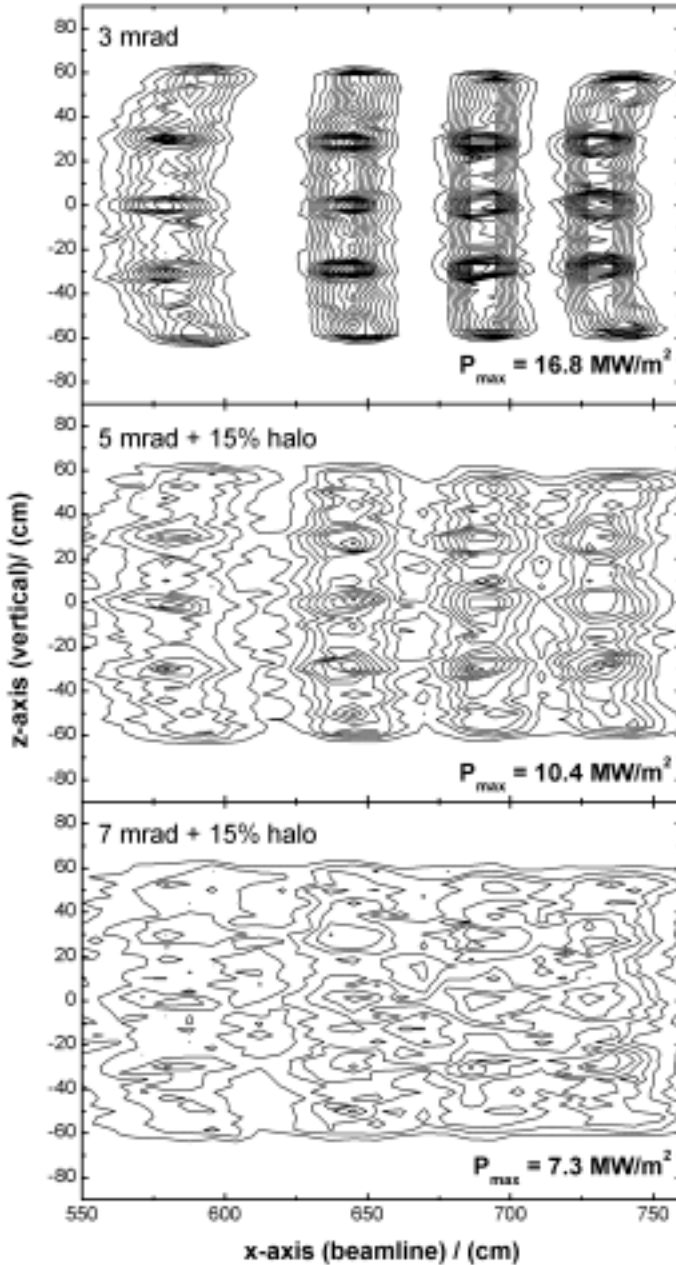


Figure 13: Power deposition profiles on the dump plates indicated in Figure 12 for a 1 MeV beam with the design parameters (see Table 1). The lines are drawn in steps on 1 MW/m^2 . The magnetic field is not screened.

Figure 14 shows the power deposition profile for the screened magnet. The beam divergence is 3 mrad. The profile is shifted in x direction compared to the unscreened case due to the lower magnetic field strength in front of the magnet. However, the maximum power density is increased by about 25% (21.3 MW/m^2 compared to 16.8 MW/m^2) due to the larger field strength within the magnet. Reducing the field strength would again result in a lower power density — and a lower stray field — but also a longer ion dump would be needed.

which is well above the value in our case (0.15 Gauss m). Furthermore, the stray field is much more important at the start of the neutralizer where all particles are still ions — and here is the stray field of the magnet zero.

The screening plates will also influence the overall pumping behavior. They divide more or less the beamline in to separate ‘chambers’. This will have consequences to the reionisation losses. Further detailed studies are necessary for optimization.

5.3 Power Deposition on the Dump Plates

Figure 12 shows the ion trajectories for both the negative and the positive residual ions, respectively. The magnet is not screened. The beam parameters are given in Table 1. The divergence is 3 mrad. The ions hit the dump plates with a maximum angle of incidence of 14° for the outermost beamlets. The corresponding power density profiles on the dump plates are shown in Figure 13. The power load can be kept below 10.5 MW/m^2 for a 5-mrad divergent beam; in the most severe case of 3-mrad divergence, there are a few hot spots up to 17 MW/m^2 . These hot spots are a result of the grid design: due to the focusing (see Table 1) there is an overlap of the beamlet groups within a column (see also Figure 3).

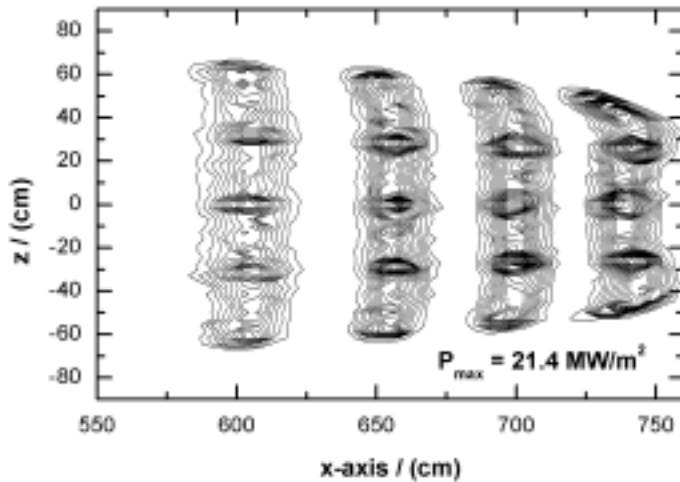


Figure 14: Power density profiles onto the target plates for a screened magnet. Lines are drawn in steps of 1 MW/m^2 . Divergence is 3 mrad , beam with design parameters.

The maximum power density MIRS has to handle is more than in the case of ERID, but in MIRS the total power is concentrated on two surfaces only, whereas in the case of ERID the total power is distributed along eight surfaces. However, the target plates of MIRS can be fed with cooling water from the backside, in contrast to the ERID swirl tubes, where the feeding has to be done from top and the cooling channels are 1.5 m long. This better cooling capacity increases the maximum acceptable power load. Most probable, sweeping will not be necessary.

In order to reduce the power density onto the target plates one might also think of a redesign of the grounded grid, optimized for MIRS, with less overlap of adjacent grid segments (see below). Also, the open structure has the advantage of an increased pumping behavior as well of a higher beam transmission (see also below). Furthermore, as already mentioned above, there is only a weak dependence of the power loads to the detailed magnet design and source geometry; hence, the MIRS design offers a large operating window for beam alignment, divergence and steering. There is a tradeoff between maximum power density and the length of the target plates. As can be seen in Figure 13, the length of the dump plates must be around 2 m , unless a detailed design of the target plates can offer a larger power handling possibility. As already remarked above, we restricted the maximum power density to about 15 MW/m^2 .

Hence, the present design needs more space — about 0.4 m to 0.5 m — than the electrostatic case. This additional space could be provided by smaller gaps between neutraliser and the magnet as well as between the target plates and the calorimeter; this may be possible due to the better pumping behavior of our open design. Constructing the field clamping at the side ‘walls’ of the magnet by iron bars instead of full area plates can furthermore increase the pumping speed within the MIRS.

5.4 Parameter studies

In the section above, we discussed a possible design for MIRS using the present grid design and the space provided for the present electrostatic ion removal system. The maximum power density the ion dumps has to handle is less than 22 MW/m^2 for the most severe case of a 3-mrad beam and a screened magnet. In this case the length of the ion dumps is about 2 m , which is 300 mm to 400 mm longer than the space allocated by ERID (see Figure 1). A shorter ion dump results in a higher power density onto the plates. Hence, the maximum power density depends on several parameters which can be chosen within the present design: (1) the beamlet divergence; (2) the length of the ion dump; and (3) the magnetic field strength.

The beamline design and the optical properties of the grid have been carefully designed in order to minimize the beam losses inside the beamline. However, as al-

ready mentioned above, the open structure of MIRS may allow a re-design of some beamline parameters. In the following section we will shortly discuss two of them: the magnet position and the focal lengths of the grid.

5.4.1 Magnet position

A result of the previous discussion was, that the length of the target plates necessary for a moderate power density exceeds the presently allocated space for the ion removal system. In order to gain more space between MIRS and calorimeter, we moved the magnet (and the target plates) towards the neutralizer by 0.3 m. On the other hand, this enables to extend the target plates; that might be necessary to decrease the power density.

The calculations show that indeed the maximum power density was reduced (not shown in this paper).

This is a consequence of the less pronounced overlap of beamlet groups if one comes nearer to the grounded grid. However, the stray field within the neutralizer increases, as can be seen in Figure 11. For the same coil current, the stray field at the neutralizer exit exceeds 50 Gauss. The best compromise between stray field, power density and target length was a reduction of the coil current to 7.5 kA instead of 9 kA. This led to a maximum power density of 19.5 MW/m² and a target end position at 7.2 m. The stray field, however, was still too high, about 20 Gauss at the exit of the neutralizer. As summary we can say that a shift of the magnet towards the neutralizer suffers from the stray field requirements within the neutralizer. Most probable, it will not be possible to position MIRS nearer to the neutralizer as it is foreseen in the present beamline design.

5.4.2 Focal lengths / Grid optics

The reference optical properties of the grid are optimized for the present beamline design. The segment and group aiming points (23.4 m each) are chosen for minimum losses in the duct, whereas especially the horizontal focal length (7.1 m) guarantees minimum beam dimensions at the exit of the present electrostatic ion dump. However, if MIRS replaces ERID, there is no need for such a focusing due to the open structure. Hence the dependence of the power load onto the target plates on the focal lengths — horizontal as well as vertical — of the grid was studied.

Figure 15 shows the maximum power density onto the target plates for a screened magnet (position at $x = 5.0$ m) as a function of the focal lengths of the grid. The design lengths are infinity for the vertical focusing and 7.1 m for the horizontal focal

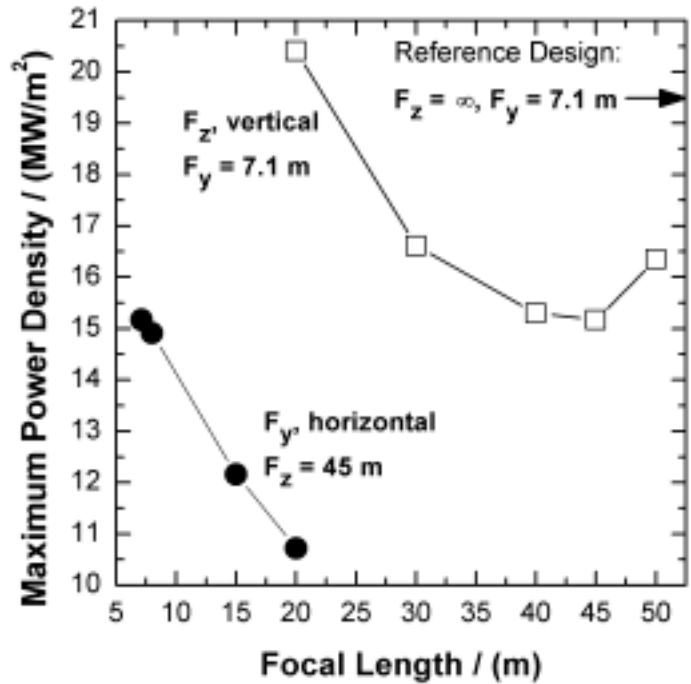


Figure 15: Maximum power density as function of the focal lengths. Zeros are suppressed. Divergence is 3 mrad; magnet position 5.0 m. Magnet is screened. For comparison, the power density obtained with the reference design lengths is indicated by the arrow.

length. It can be seen in the figure, that the maximum power density can be drastically reduced by a factor of 2. A change of the vertical focal length results in a reduction of 20% — the minimum being at 40-45 m — compared to the maximum power density for the design focal lengths, whereas the main reduction comes from a change of the horizontal focal length.

Figure 16 shows the resulting power density profile for the more realistic case of a magnet position of 5.3 m. Here vertical and horizontal focal lengths of 40 m and 20 m, respectively, are chosen. The power density profile is much more broadened compared to the profile obtained with the design parameters (Figure 14) resulting in a factor of 2 reduction of the maximum power density.

The horizontal focal length of 7.1 m of the design — this is at the end of the electrostatic residual ion dump — nearly maximizes the power density in the overlap region of the beam segments. Hence, shifting the horizontal focal length towards the duct — and hence towards the group and segment aiming point — results in a wider spread of the power along the beam; as it can be seen in Figure 16, the overlap regions nearly disappeared.

Hence, despite the fact that the total power onto the target plates remains the same — i.e. $0.2 \times 40 \text{ MW} = 8 \text{ MW}$ —, the cooling is much easier due to the more distributed power; the hot spots with power densities around 20 MW/m^2 disappeared. For a divergence of 5 mrad a 50% reduction of the power density will result in a power density below 6 MW/m^2 , below this limit even swirl tubes can be used as target plates. On the other hand, the reduction of the power density by changing the grid optics can be partly overturned by increasing the magnetic field. This will of course result in an increase of the power density, but — and this is important — in a shorter target plate.

A change of the optical properties of the grid may affect the losses of the beam at the different beamline components and it will affect the beam properties in the main plasma of the ITER tokamak.

Table 2.1. compares the losses in the neutralizer and the duct for our ‘best’ focusing with the design values. The losses increase in the neutralizer for the larger focal lengths. For a 5 mrad beam the losses are more than 6 MW, which is certainly too high. However, the neutralizer was designed to be adapted to the design grid focusing. If MIRS with different beam optics is chosen, the neutralizer — and the whole beamline design — has to be re-optimized.

Table 2.2. compares the maximum power density onto the (closed) calorimeter. As it is already the case for the MIRS ion target plates, the maximum power the calorime-

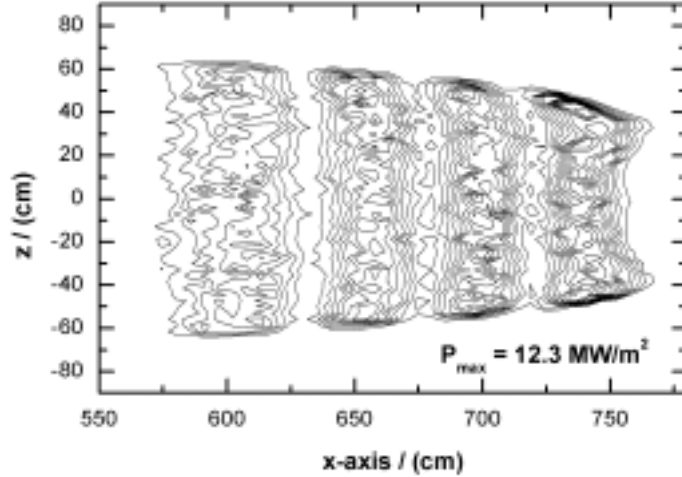


Figure 16: Power density onto the target plates for vertical and horizontal focal lengths of 40 m and 20 m, respectively. Lines are drawn in steps of 1 MW/m^2 . Divergence is 3 mrad, magnet position is 5.3 m and screened. For a comparison to the focal lengths of the reference design see Figure 14.

Table 2: Beam losses at various beamline components, maximum power densities onto the calorimeter and maximum beam power densities for different focusing and divergences. Geometrical transmission is neglected; only neutralization fraction (0.6) is taken into account.

	Reference	Design Focus	'Best' Focus	
		$F_z = \infty$ $F_y = 7.1$ m	$F_z = 40$ m $F_y = 20$ m	
Divergence:	3 mrad	5 mrad	3 mrad	5 mrad
1. Beam losses (MW):				
Neutralizer:	0.08	3.92	0.72	6.46
Duct:	0	0.33	0.004	0.36
2. Maximum Power Density (MW/m²): (total power 24 MW)				
Calorimeter:	17.3	11.3	15.2	10.3
3. Maximum Beam Power Density (MW/m²):				
Neutralizer (total power 40 MW):				
Entrance	159	143	129	133
Exit	372	173	168	131
Calorimeter (total power 24 MW):				
Entrance:	210	115	120	87
Duct (total power 24 MW):				
Exit:	357	253	1165	462

ter plates have to handle decreases using our focusing parameters. The reason is the same: the reduction of the power density in the overlap regions within the groups.

The maximum beam power density at the various positions of the beamline is summarized in Table 2.3. The reduction of the maximum power density can be seen clearly within the beamline, which is reflected in the reduction of the maximum power densities at the main target plates (ion dump, calorimeter). However, the beam power density at the duct exit, and hence also at the separatrix, is increased by a factor of 3. This is due the fact that the horizontal focal length of 20 m in our case is nearly the same as the group/segment aiming point (23.4 m) at the duct exit. The corresponding neutral beam power density profiles are shown in Figure 17. For a correct comparison, it is assumed that the overall transmission is 1, and only the neutralized fraction is taken into account. Due to the longer horizontal focal length, the beam is much more concentrated reducing the duct losses and increasing the power density. This might be an advantage or a disadvantage for the heating: the power deposition profile is more localised and the shinethrough power density is increased.

6 Beamline Transmission

(by H.P.L De Esch)

The transmission to ITER is calculated for several variations on the reference design of ITER. The accelerator for the neutral beam system proposed for ITER must accelerate 40 A of D^- to 1 MeV for up to 3600 s. The European concept, the SINGle GAP, SINGle APerture (SINGAP) accelerator is an attractive alternative to the reference design, the so-called Multi-Aperture, Multi-Grid (MAMuG) accelerator, which is being developed in Japan. A perveance scan done (on the computer) for both systems defines for each current density j_D^- the divergence and steering direction of each of the 1280 beamlets that have been accelerated through either system.

The MAMuG system accelerates the beamlets individually through 7 multi-aperture grids. The beamlets are steered by bending the accelerator grids in two dimensions to achieve the correct aiming to the duct exit, offsetting individual apertures to obtain focusing at the exit of the reference electrostatic RID and it might even need small kerbs on individual apertures. The SINGAP pre-accelerates the 1280 beamlets individually through 3 multi-aperture grids to ~20-50 keV. The acceleration to 1 MeV is done in a single step, using a grounded grid containing 16 very large apertures, called “hyperapertures”. Each of the hyperapertures corresponds to a beamlet group from the 4x4 matrix. The system relies on flat grids without aperture offset steering by the pre-accelerator grids. Groups of beamlets are steered by offsetting the hyperapertures in the grounded grid. In MAMuG, the steering of each individual beamlet is controlled. In SINGAP, the steering of each 5x16 beamlet group is controlled. To counteract the space-charge repulsion between individual beamlets, a so-called kerb is fitted to the pre-acceleration grid around each group of beamlets. The systems are described in [19]; a good additional reference for SINGAP is in [20]. A schematic picture of the ITER neutral beam injector used for the transmission calculations is shown in Figure 18. The segmented reference RID is in

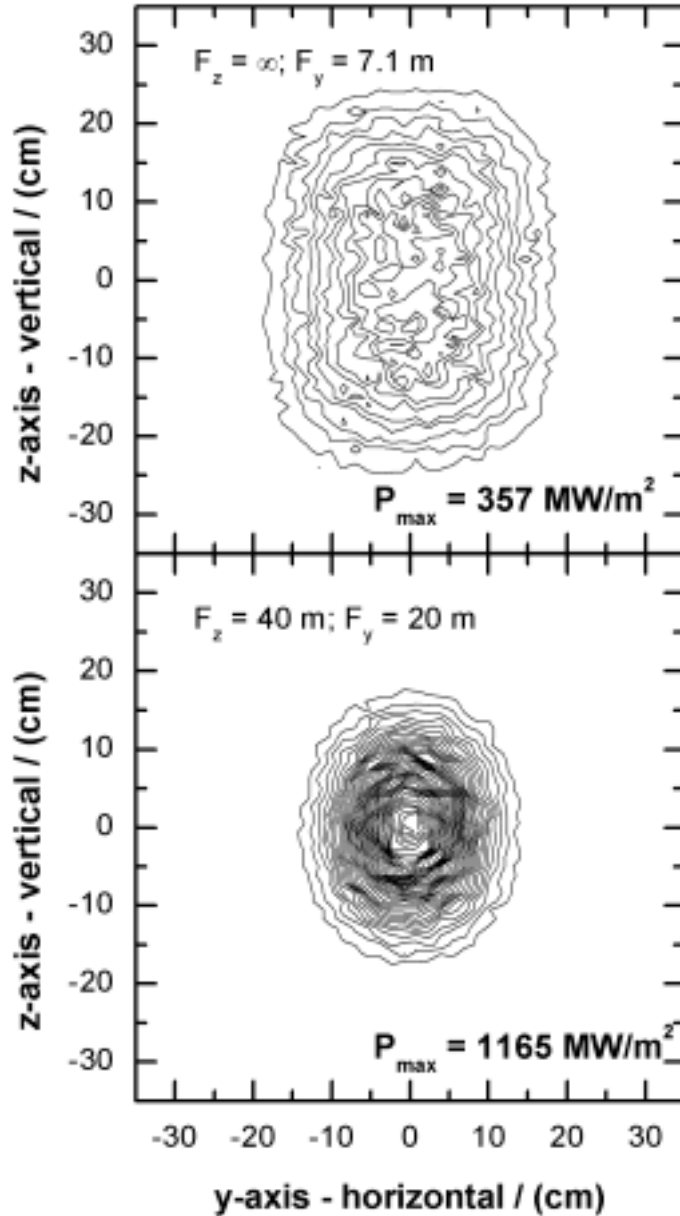


Figure 17: Neutral beam profiles at the exit of the duct ($x = 23.4$ m) for ITER reference design focusing (top) and our ‘best’ focusing (bottom). Divergence is 3 mrad. The lines are drawn in steps of 30 MW/m^2 . The total power is 24 MW.

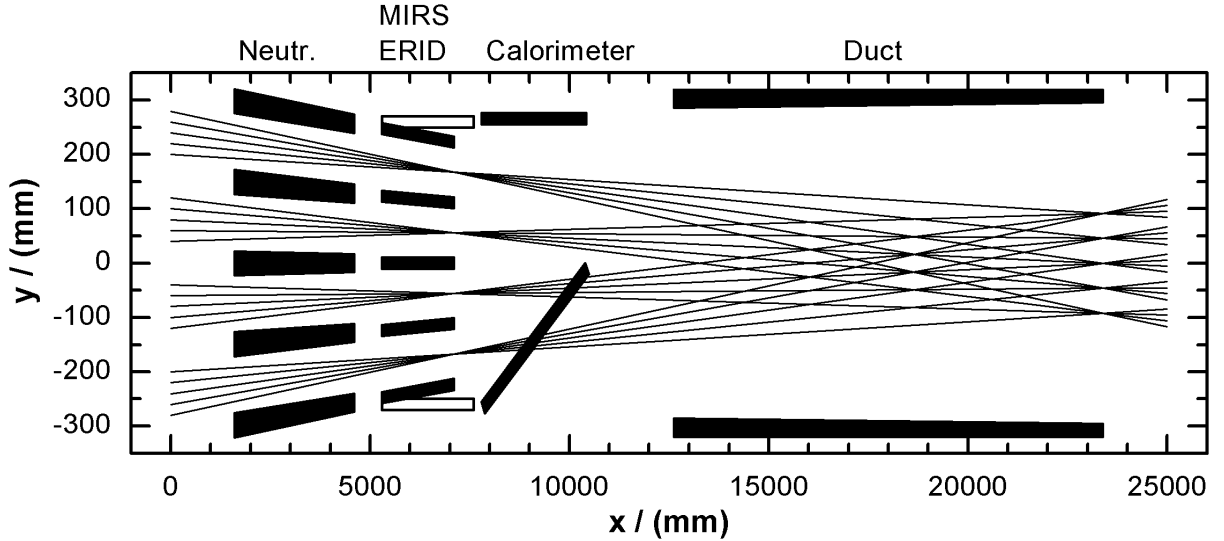


Figure 18: Horizontal cross-section of the beamline on ITER, showing the aiming of the 4 beam columns through the segmented neutraliser and ERID (closed rectangles) or MIRS (open rectangles), respectively,, then through the calorimeter and the long duct towards ITER. For illustration purposes is one half of the calorimeter drawn in the open position, the other half in the closed position. The divergence of the beamlets shown is zero. Note the different scaling of the y- and the x-axis, respectively.

blue and the alternative magnetic RID is in red. Only one RID will be installed: either the blue or the red.

On the 23.4 meter way to the ITER tokamak, the accelerated beam has to go past a segmented neutraliser (presenting an opening that is 94 mm wide at a distance of 4.6 meter; 10.2 mrad), a residual ion dump (RID) and a duct that presents an opening of 582 mm at the tokamak first wall (12.4 mrad). The reference RID is segmented like the neutraliser and presents a 90 mm wide opening located 7.1 meters from the accelerator (6.3 mrad).

The MIRS system is not segmented (open) and presents a 500 mm wide opening to the beams (35 mrad). Due to the finite size of the beam source and the various steerings, the full angle indicated is not (always) available to the beams, but it gives an indication. A significant gain in transmission can be expected if the reference RID would be replaced by the magnetic RID, because the 6.3 mrad acceptance angle by the reference design is the most limiting.

6.1 Perveance scans

Perveance scans (variation of the extracted current density, while keeping all the voltages in the acceleration system constant) have been carried out for SINGAP [20], [21] and MAMuG (this report). The geometry and voltages for the MAMuG stack have been obtained from [1]; then a perveance scan was performed using SLAC.

The SLAC code could reproduce the quoted performance and in fact predicted even a slightly lower divergence ($0.14^\circ = 2.4 \text{ mrad}$). For SINGAP it was found in [21] that the beamlets would touch the pre-acceleration grid for $j_{\text{acc}} > 24 \text{ mA/cm}^2$. Here we find for MAMuG that the electron suppression grid is touched for $J_{\text{acc}} > 23 \text{ mA/cm}^2$. The re-

Table 3: SLAC perveance scan on MAMuG

J_{source} (mA/cm ²)	$J_{\text{accelerated}}$ (mA/cm ²)	Divergence (mrad)
30.3	23	3.0
26.3	20	2.4
22.4	17	3.3
18.4	14	4.7

sults for the MAMuG perveance scan are summarized in Table 3. All calculations take the stripping losses into account.

For MAMuG, the result of a perveance scan is a set of different divergences that correspond to a set of current densities. The steering angle of the beamlets is not affected as it is determined by the position of

the apertures in the 7 grids.

For SINGAP, as described in [21], not only different divergences result for each current density, but also different beamlet steering angles. These steering angles are different for each chosen current density because the kerb is designed for one particular current density and acceleration voltage combination (typically 20 mA/cm², 1 MV). SINGAP hyperbeamlets have the useful property that the edge converges inwards, while the core diverges. This feature is more advantageous with an open RID than with a segmented one. All these effects have been taken into account for the transmission calculations. (These different beamlet steering angles affect the power deposition profiles on the MIRS target plates; a detailed study is necessary if MIRS together with SINGAP is chosen.)

The properties of the 1280 accelerated beamlets (position, diameter, divergence, aiming) were fed into TRANSMIT. This program calculates the power deposition on a test plane by adding the power density from all the beamlets (assumed to be Gaussian) on each point of the test plane. The code checks if a particular beamlet is screened by one of the scrapers that are defined. All beam-scraping surfaces in Figure 18 have been input to TRANSMIT, assuming that the calorimeter is open, of course. Calculations have been done with the reference RID (blue in Figure 18) enabled or with the alternative RID (red in Figure 18) enabled.

Because a code calculation is always idealized in some way (source uniformity, ion temperature, magnetic field deflections, grid distortions, etc.), an extra 2 mrad is added to the divergence of each beamlet. Moreover, a random extra divergence between 0 and 1 mrad is added to the divergence of each beamlet. Also a random angle between -1 and +1 mrad is added to the starting angle of each beamlet. This is done to make the results more 'realistic'

6.2 Results of the calculations

The results of all the calculations are in Figure 19. It shows the geometrical transmission to ITER in percent for MAMuG and SINGAP, in combination with either the reference electrostatic segmented RID or the alternative magnetic open RID. It can be seen that the transmission to ITER increases significantly when the segmented RID is replaced by an open RID and the geometrical transmission becomes close to 100%, even at off-normal beam-optics performance. The gain in transmission due to an open RID is around 10% for optimum beam parameters and significantly more for non-optimum parameters.

The total injected power will increase by about 1.7 MW per beamline at the nominal values (i.e. for a 3 mrad beam with the reference design focal lengths). However,

Table 2.1. shows, that in the case of our 'best' focusing — and especially in the case of a 5 mrad beam — this gain in the injected power due to the open structure of MIRS is wasted at the neutralizer. Hence, a re-optimization of the neutralizer design as well of the whole beamline is necessary if different beam optics is chosen. Then the transmission and the injected power might be further increased. Figure 19 shows also — as it is the case for the power deposition on the target plates — that the open structure of MIRS again shows a certain robustness of the transmission against changes of divergence and misalignment.

With the designs as they are now, SINGAP is slightly better 'optimized' for MIRS than MAMUG. There is however no reason why should that be the case after a re-optimization of both concepts for MIRS.

7 Summary

In this paper we present an alternative design for the ion removal system of the ITER NBI. The ions are deflected by a vertical magnetic field to two in-line dump plates. The maximum power density deposited onto the target plates is well below 15 MW/m² with an optimized grid optic design.

This concept has several advantages over the reference design of an electrostatic deflection to in-line target plates forming four narrow channels:

- increased beamline transmission and hence, an increased injected power (1.7 MW per beamline at the reference value for a 3 mrad beam with the reference design parameters),
- wide operation window regarding beam alignment, divergence and steering,
- robustness against changes in the neutralizer target thickness, changing the balance of positive and negative residual ions,
- and no accelerated secondary electrons.

On the other hand, MIRS creates an additional stray field that has to be compensated and the maximum power load is higher than in the case of ERID. But this can be handled by the better access to the target plates for the cooling (from the back in-

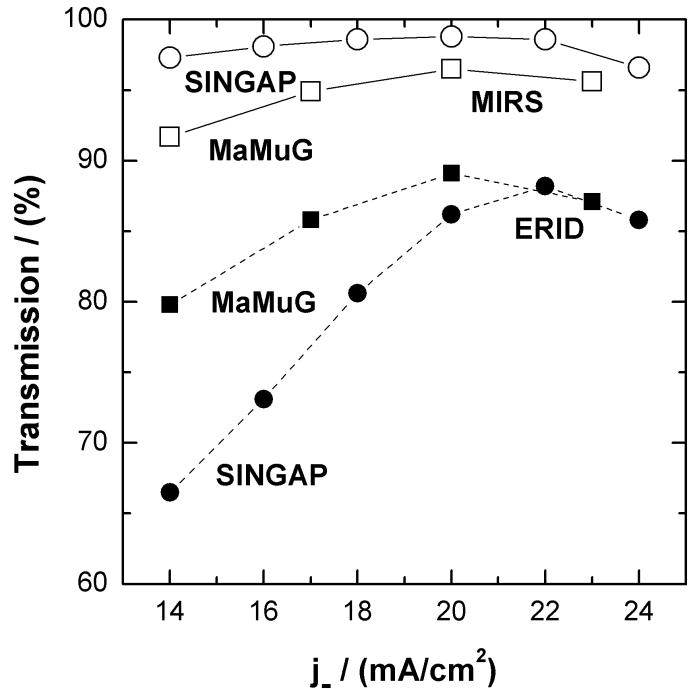


Figure 19: Geometrical transmission of the ITER neutral beamline for a 1 MeV beam vs. accelerated current density for the different acceleration systems — SINGAP (circles) and MAMUG (squares), respectively — and the different ion removal systems — MIRS (open symbols) and ERID (closed symbols), respectively.

stead from top). Furthermore, the presence of coils in a high-level neutron radiation field may cause additional problems.

The present design exceeds the allocated length of the reference design by 0.2 to 0.3 m. But the better pumping behavior of MIRS could ease the need for pumping gaps between the beamline components that can then provide the additional few 100 mm needed. On the other hand the reduction of the power density due the optimized grid optics offers more freedom in shortening the target plate length.

If MIRS is chosen for the ion removal system of ITER, a redesign of the grip optics and the whole beamline — especially the beam limiting components as the neutralizer and the duct — is essential in order to optimize the beam losses, the gas flows and the power densities at the high heat flux components of ion dump and calorimeter — and perhaps the deposition profile in the plasma.

References

- [1] Technical Basis for the ITER Design, ITER EDA Documentation series, to be published from IAEA, Vienna.
- [2] O. Vollmer, A. Stäbler, E. Speth, M. Ciric, P. Franzen, B. Heinemann, W. Kraus, W. Melkus, R. Riedl, W. Schärlich. Commissioning and performance of the new ASDEX Upgrade neutral beam injector. Proc. 20th Symp. Fusion Technology, EURATOM-CEA, Saint Paul lez Durance 1998, p. 449
- [3] A. Stäbler, O. Vollmer, J.H. Feist, E. Speth, B. Heinemann, W. Melkus, S. Obermayer, R. Riedl, W. Schärlich, K. Wittenbecher. Performance of the first ASDEX Upgrade neutral beam injector. Fusion Technology 1994. Proceedings of the 18th Symposium on Fusion Technology. Elsevier. Part vol.1, 1995, pp.593-6 vol.1. Amsterdam, Netherlands.
- [4] F.P. Penningsfeld, J.H. Feist, K. Freudenberger, W. Ott, E. Speth. Commissioning and first operation of the W VII-AS neutral beam system. Proceedings of the IEEE Thirteenth Symposium on Fusion Engineering (Cat. No.89CH2820-9). IEEE. 1990, pp.288-91 vol.1. New York, NY, USA.
- [5] G. Düsing, H. Altmann, H. Falter, A. Goede, R. Haange, R.S. Hemsworth, P. Kupschus, D. Stork and E. Thompson, Neutral Beam Injection System. Fusion Technology 11 (1987) 163
- [6] L.R. Grisham et al., Nucl. Instr. and Methods B10/11 (1985) 478
- [7] S. Matsuda et al., Fusion Engineering and Design, 5 (1987) 85
- [8] A.P. Colleraine et al., Proc. 11th Symp. on Fusion Engineering, Vol. 2, (IEEE New York 1982) 1278
- [9] O. Kaneko et al., Development of negative-ion-based neutral beam injector for the large helical device, NIFS-441, Sept 1996, 16th IAEA Fusion Energy Conf, 7-11 Oct 1996, Montreal (CAN)
- [10] M. Kuriyama et al., Negative-ion based neutral beam injector for JT-60U, 18th SOFT, Karlsruhe, Aug 22-26, 1994
- [11] Ph. Lotte, JDC Meeting, Cadarache, 1996
- [12] A. Panasenkov, ITER Review Meeting on Neutral Beams, Naka, May 2001

- [13] E. DiPietro, Internal Memorandum, IDoMS - N53 MD 32 99-08-13 W 0.1
- [14] A. Stähler, J. Sielanko, S. Götz, E. Speth. Computer-Simulation of the Reionisation Effects for the ASDEX-Upgrade Neutral Beam Injector. *Fusion Technology* 26(2) (1994) 145
- [15] W. Müller, *Archiv für Elektrotechnik* 69 (1986) 295
- [16] J.H. Feist, S. Götz and J. Sielanko, Proc. of the 14th SOFT, Avignon (1986) 1121
- [17] J.H. Feist, A. Stähler, J. Dunne, K. Freudenberger, B. Heinemann, R. Riedl, J. Sielanko, and E. Speth. Performance of the Ion Removal System for the ASDEX Upgrade Neutral Beam Injectors. Proc. 17th SOFT, Rome (1992)
- [18] P. Franzen, J. Sielanko, R. Riedl, E. Speth, *Fusion Engineering and Design*, vol. 56-57, 2001, p 511
- [19] DDD5.3 in the ITER final design report, 2001, on a shiny disc, unavailable.
- [20] H.P.L. de Esch, R.S. Hemsworth and P. Massmann, *SINGAP, The European concept for negative ion acceleration in the ITER neutral injectors*. *Review of Scientific Instruments* 73(2002)1045.
- [21] H.P.L. de Esch and R.S. Hemsworth, *SINGAP (ITER) perveance scan*, Internal DRFC/GIDN note dated 3 April 2001